



UNIVERSITÀ
DEGLI STUDI
FIRENZE

FLORE

Repository istituzionale dell'Università degli Studi di Firenze

Virtual incidence effect on rotating airfoils in Darrieus wind turbines

Questa è la Versione finale referata (Post print/Accepted manuscript) della seguente pubblicazione:

Original Citation:

Virtual incidence effect on rotating airfoils in Darrieus wind turbines / Bianchini, Alessandro; Balduzzi, Francesco; Ferrara, Giovanni; Ferrari, Lorenzo. - In: ENERGY CONVERSION AND MANAGEMENT. - ISSN 0196-8904. - ELETTRONICO. - 111:(2016), pp. 329-338. [10.1016/j.enconman.2015.12.056]

Availability:

This version is available at: 2158/1017690 since: 2021-03-30T14:34:54Z

Published version:

DOI: 10.1016/j.enconman.2015.12.056

Terms of use:

Open Access

La pubblicazione è resa disponibile sotto le norme e i termini della licenza di deposito, secondo quanto stabilito dalla Policy per l'accesso aperto dell'Università degli Studi di Firenze (<https://www.sba.unifi.it/upload/policy-oa-2016-1.pdf>)

Publisher copyright claim:

(Article begins on next page)

Virtual incidence effect on rotating airfoils in Darrieus wind turbines

Alessandro Bianchini^{1a}, Francesco Balduzzi^{1b}, Giovanni Ferrara^{1c}, Lorenzo Ferrari^{2d}

¹⁾ Department of Industrial Engineering, University of Florence
Via di Santa Marta 3, 50139, Florence, Italy
Phone +39 055 275 8773

³⁾ CNR-ICCOM, National Research Council of Italy
Via Madonna del Piano 10, 50019, Sesto Fiorentino, Italy
Phone +39 055 5225 218 - Fax +39 055 5225 203

Abstract

Small Darrieus wind turbines are one of the most interesting emerging technologies in the renewable energies scenario, even if they still are characterized by lower efficiencies than those of conventional horizontal-axis wind turbines due to the more complex aerodynamics involved in their functioning. In case of small rotors, in which the chord-to-radius ratios are generally high not to limit the blade Reynolds number, the performance of turbine blades has been suggested to be moreover influenced by the so-called “flow curvature effects”. Recent works have indeed shown that the curved flowpath encountered by the blades makes them work like virtually cambered airfoils in a rectilinear flow.

In the present study, focus is instead given to a further effect that is generated in reason of the curved streamline incoming on the blades, i.e. an extra-incidence seen by the airfoil, generally referred to as “virtual incidence”. In detail, a novel computational method to define the incidence angle has been applied to unsteady CFD simulations of three airfoils in a Darrieus-like motion and their effective angles of attack have been compared to theoretical expectations.

The analysis confirmed the presence of an additional virtual incidence on the airfoils and quantified it for different airfoils, chord-to-radius ratios and tip-speed ratios. A comparative discussion on BEM prediction capabilities is finally reported in the study.

Keywords: Darrieus, vertical axis wind turbine, flow curvature, virtual incidence, CFD, angle of attack, BEM

1. Introduction

Increasing interest is presently being paid to understand where, beyond large wind farms, small and medium-size wind turbines can represent an alternative for delocalized power production [1], with particular focus on off-grid applications (e.g. [2-3]). *Inter alia*, the built and populated environment presently represent the research frontier [4], since the produced power could be immediately available for a large number of applications or simply used to reduce the energy demand of buildings [5]. Even in the flows in this environment are generally very complex, if properly positioned small turbines are thought to take advantage from augmented wind speeds [6] or specific interactions with the buildings [7].

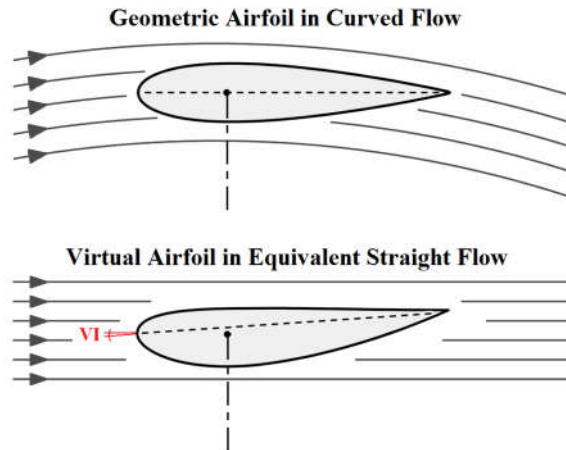
a) bianchini@vega.de.unifi.it
c) giovanni.ferrara@unifi.it

b) balduzzi@vega.de.unifi.it
d) lorenzo.ferrari@iccom.cnr.it (*=corresponding author)

42 Among other technologies, Vertical-Axis Wind Turbines (VAWTs), both drag (e.g. [8-9]) and
 43 lift-driven (e.g. [10-11]), are gaining popularity in view of similar applications, since they can work
 44 effectively even in presence of low-speed and unstructured flows with low noise emissions and high
 45 reliability [12]. In particular, Darrieus rotors are increasingly appreciated, as they are probably the
 46 only ones able to reach efficiencies somehow competitive with respect to Horizontal-Axis Wind
 47 Turbines (HAWTs) [13]. Moreover, differently from HAWTs, they are supposed to even improve
 48 their power coefficient in case of skewed flow [14-15].

49 At the present state-of-the-art, however, the global efficiencies of Darrieus turbines still lack
 50 from those of HAWTs, due to their intrinsically more complex aerodynamics coming from the
 51 revolution of blades around an axis orthogonal to flow direction. This generates a continuous
 52 variation of the angle of attack, which leads to additional phenomena, like for example dynamic
 53 stall [13].

54 Recently, a study by Bianchini et al. [16] demonstrated that the so-called “flow curvature
 55 effects” represent one of the main aspects to be assessed in order to achieve a deeper understanding
 56 of Darrieus turbines’ aerodynamics. The first studies on these phenomena date back to the early
 57 ‘90s, when Migliore et al. [17], based on a one-dimensional analysis of the attended velocity vectors
 58 along the airfoil, theorized that the curved path VAWT blades follow imparts a *virtual camber* and
 59 a *virtual incidence* on them, i.e. that their performance would be analogous to that of a cambered
 60 blade at modified incidence in a rectilinear flow (see Fig. 1). Migliore and his colleagues anyhow
 61 theorized these effects only using non-dimensional theories and did not verified it on real turbines.
 62



63
 64 **Figure 1 - Flow curvature effects on an airfoil in Darrieus-like motion.**
 65

66 A recent work published by the authors have shown that the associated differences in
 67 performance between “geometrical” and “virtual” airfoils become a source of error in any analysis
 68 using the original blade profile’s data [18]. Their attention was however fully focused on the virtual
 69 camber effect.

70 This study sets out instead to both assess the presence of the virtual incidence and to estimate its
 71 impact on airfoil’s performance in order to judge how best account for it in low-order simulation
 72 methods, like Blade Element Momentum (BEM) codes.

73 To do so, the same three airfoils analyzed in Ref. [18] were considered, i.e. a conventional
 74 symmetric NACA 0018 and two modified profiles based on it. In details, the two modified profiles
 75 have been conformally transformed to fit their camber lines to the arc of a circle, such that the ratio
 76 between the airfoil chord and the circle’s radius, c/R , is 0.114 or 0.25 (Fig. 2).
 77

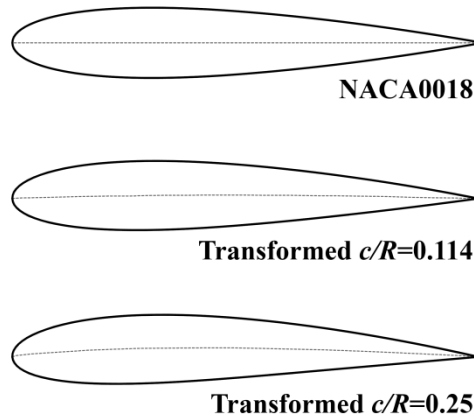


Figure 2 – The three profiles used in this study.

78
79
80

81 The two c/R values were selected as compatible with the ones originally used by Migliore [17],
82 whose theory was used as a comparison in the present study. Based on the applied transformations,
83 the $c/R = 0.114$ airfoil has a maximum camber of 1.42% at 50% of chord, while the $c/R = 0.25$ has
84 3.11% maximum camber, again at 50% of chord. Following the indications of Ref. [18], it has to be
85 attended that “in tunnel-like flow condition the transformed airfoils should perform as the
86 unmodified NACA 0018 would in VAWTs with similar c/R ratios and conversely the NACA
87 0018’s results in rectilinear flow should correspond to those of the transformed airfoils when used
88 in the VAWTs” [18].

89 To analyze the airfoil’s behavior and then estimate the actual incidence they are experiencing,
90 CFD simulations have been carried out at different tip-speed ratios and analyzed in terms of
91 incidence angles experienced by the profiles using a novel method developed by the authors [19].

92 2. Case study and CFD simulations

93 CFD simulations were used to investigate the aerodynamic behavior of the selected airfoils when
94 rotating onboard a Darrieus turbine. The use of CFD to go into the aerodynamics details of the
95 phenomena and then define proper corrections to be transferred to low-order simulation methods is
96 indeed a recent trend in the research, which is disclosing very interesting horizons for a further
97 comprehension of many details of airfoils’ functioning (e.g. [20-21]).

98 Four “single-bladed” rotors were considered, obtained by combining the two c/R ratios with both
99 the NACA 0018 and the relevant transformed airfoils in each case.

100 Table 1 reports the main geometrical features of the four simulated models. The airfoil chord
101 was kept constant in all the simulations, while the revolution radius was changed to achieve the two
102 desired chord-to-radius ratios.

103
104

Table 1 – Test cases.

	Case 1	Case 2	Case 3	Case 4
c/R	0.114		0.25	
airfoil	NACA0018	Transformed ($c/R=0.114$)	NACA0018	Transformed ($c/R=0.25$)
c [m]	0.20	0.20	0.20	0.20
R [m]	1.75	1.75	0.80	0.80
U [m/s]	8.0	8.0	8.0	8.0

105
106
107
108

The authors have presented in recent works [22-23] the assessment and validation of the main numerical settings that have been used in CFD simulations. The validity of these settings has been verified by comparing simulations to several experimental data, both in terms of power coefficient

109 vs. tip-speed ratio and of torque profile during the revolution [20], obtaining a constant and very
110 satisfactorily agreement. For completeness, the main settings are anyhow briefly summarized here.

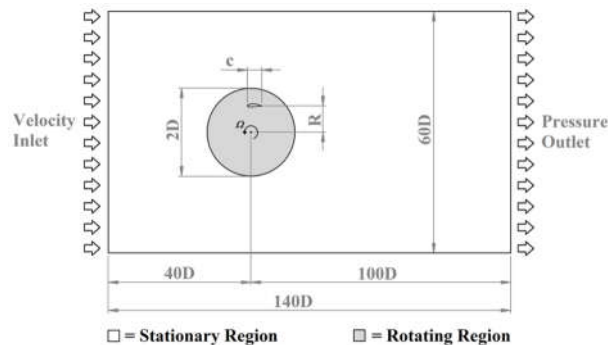
111 The commercial code ANSYS Fluent [24] was used for the 2D simulations, which made use of a
112 time-dependent unsteady Reynolds-averaged Navier-Stokes (U-RANS) approach, in the pressure
113 based formulation. The Coupled algorithm was employed to handle the pressure-velocity coupling.
114 A dedicated sensitivity analysis [22] and recent studies from the literature [25] indeed showed that
115 this algorithm ensured more robust results when adopting different meshes, timesteps, or rotating
116 speeds. The second order upwind scheme was used for the spatial discretization of the whole set of
117 RANS and turbulence equations, as well as the bounded second order for time differencing to
118 obtain a good resolution [22].

119 Air was modeled as an ideal compressible gas with standard ambient conditions, i.e. a pressure
120 of 1.01×10^5 Pa and a temperature of 300 K.

121 The global convergence of each simulation was monitored by considering the difference between
122 the mean values of the torque coefficient over two subsequent revolutions normalized by the mean
123 value over the second period of the pair. The periodicity error threshold was set to 0.1% [22].

124 Exploiting the sliding-mesh model of the solver, the simulation domain was divided into two
125 subdomains in order to allow the rotation of the turbine, as proposed by Maître et al. [26] and Raciti
126 Castelli et al. [27]. Fig. 3 shows a circular zone containing the turbine, with a diameter ($2D$) twice
127 that the turbine itself (D). R represents the turbine radius. The circular zone rotates with the angular
128 velocity of the rotor while a rectangular fixed outer zone determines the overall domain extent.

129 The final dimensions of both domains (reported in Fig.3) were defined according to the
130 sensitivity analysis reported in [22] in order to allow a full development of the turbine wake.
131



132
133 **Figure 3 – Simulation domain.**
134

135 The mesh settings were defined accordingly to the results of the grid-independency analysis
136 reported in [22], where six different levels of refinement of the mesh were tested. An unstructured
137 mesh composed by triangular elements was used for the discretization of the core flow region,
138 whereas the entire boundary layer region has been described with a structured O-grid of 50 layers.

139 Based on the requirements of the selected turbulence model, the first cell height was selected as
140 to provide a dimensionless wall distance (y^+) during the rotor revolution constantly lower than 1.

141 The expansion ratio for the growth of elements starting from the surface was kept below 1.1 to
142 achieve good mesh quality in proximity of the airfoil.

143 Based on [22], the airfoil was discretized with approximately 600 nodes. As a result, the mesh
144 size of the rotating region, for the single-bladed configuration, results in approximately 1.4×10^5
145 elements, while the stationary region is discretized with 2.0×10^5 elements. Figures 4 and 5 show
146 some details of the grids. The mesh is refined in the region surrounding the blade due to the higher
147 complexity of the flow field. As suggested by [27] and recently demonstrated by [28], a *control*
148 *circle* (Fig. 4a), with a diameter equal to twice the airfoil's chord, was defined around the blade in
149 order to have a better capability to control the elements size in the region closer to the blade itself.
150

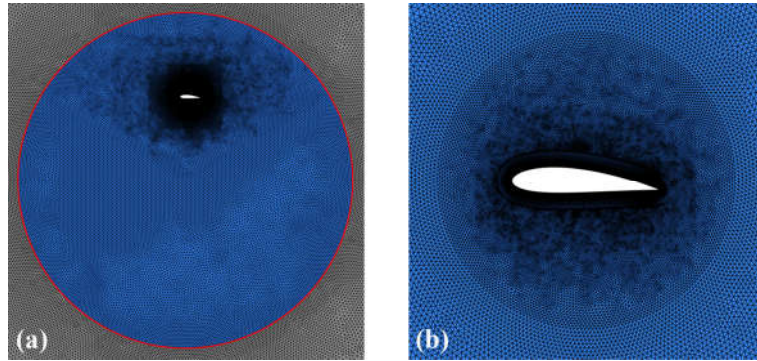


Figure 4 – Computational grid for the rotating domain (a) and control circle details (b) for transformed airfoil with $c/R=0.25$.

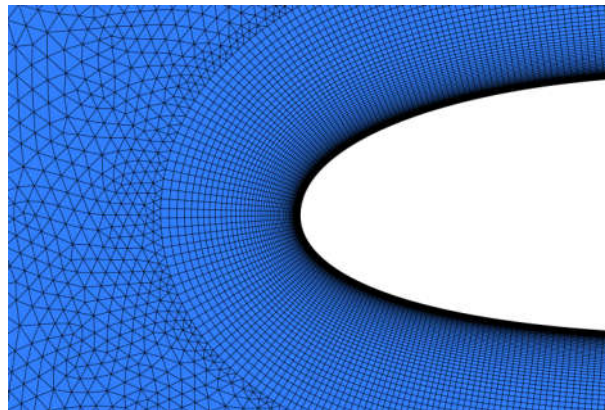


Figure 5 – Computational grid: boundary layer discretization at the leading edge (e.g. transformed airfoil with $c/R=0.25$).

Recent work [22] demonstrated that, in case of Darrieus VAWTs, different functioning TSRs require specific minimum timesteps of CFD simulations in order to ensure accurate results throughout the entire power curve. According to [22], in the present analysis angular timesteps in the range between 0.135° and 0.42° were used, corresponding to the cases with the lowest and the highest TSR respectively.

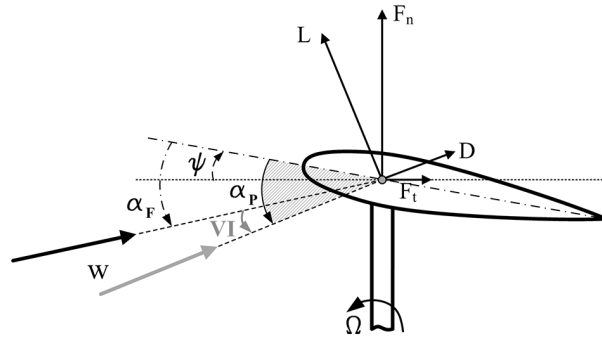
Concerning the turbulence closure problem, Balduzzi et al. [23], showed the effectiveness of Menter's shear stress transport (SST) [29] model in performance simulations involving unsteady aerodynamics for VAWTs, as also confirmed by wide use in literature. In the present study, however, attention has been focused on a more detailed examination of the aerodynamic behavior of each single airfoil in motion by analyzing equivalent static pressure coefficients on the blade profiles. Since the prediction of the boundary layer evolution becomes a critical issue and the blade Reynolds number for the considered cases cannot guarantee a fully turbulent condition, the $\gamma-Re_\theta$ transition model (derived by Menter and Langtry from the SST model [30]) was implemented, despite its increased computational cost. Lanzafame et al. recently showed good agreement between experimental data and numerical results obtained with the transition turbulence model for two different types of H-Darrieus turbines [31].

3. Data analysis

The main concern of the present study is to assess and quantify the virtual incidence (VI) seen by the airfoils in motion onboard Darrieus wind turbines.

According to the original work by Migliore, the virtual incidence is defined in Fig. 6 as the difference between the angle of attack really experienced by the airfoil α_P (i.e. that matching the

180 airfoil's performance in straight flow) and the flow angle (i.e. the angle between the relative
 181 velocity and the airfoil's chord) in the same point α_F (Eq.1). The angle ψ represents the hypothetical
 182 pitch angle between the chord and the tangential direction.
 183



184
 185 **Figure 6 – Definitions and graphical convention.**

186
$$\alpha_P = \alpha_F + \psi \quad (1)$$

187 In the first estimation by Migliore [17], the flow angle was simply calculated by resolving the
 188 velocity triangle composed by the peripheral speed and the undisturbed wind velocity (no induction
 189 factor was even provided). On the other hand, the incidence “seen” by the airfoil was estimated
 190 accounting for the local angle between the flow direction and the airfoil’s surface along the chord.

191 In the present study, both components have been estimated from CFD with two novel
 192 approaches, in order to achieve a much higher degree of confidence on the results and then on the
 193 estimation of the virtual camber. To do so, once each simulation had reached full convergence, the
 194 pressure distribution over the airfoil and the flow field in proximity of the blades were acquired
 195 approximately every 1.5 degrees of azimuthal increment [32].
 196

197 **3.1 Definition of the angle of attack (AoA) and relative speed modulus**

198 In order to investigate the virtual incidence acting on the airfoils, a robust procedure to
 199 extrapolate the angle of attack was first needed. This is not an automatic procedure as the concept of
 200 incidence angle actually belongs to one-dimensional aerodynamics and cannot be directly
 201 transferred to a real flow.

202 The concern of defining the angle of attack from CFD simulations of rotating blades has been
 203 originally addressed by wind turbine specialists in case of HAWTs [33]. In case of Darrieus
 204 VAWTs, where the AoA changes constantly during the revolution and the streamline are deflected
 205 due to curvature, the definition of an incidence angle is even more complex. Recently, the authors
 206 have proposed a novel methodology to extrapolate the AoA from 2D CFD simulations of a Darrieus
 207 turbine [19] and have successfully applied it to the study of the virtual camber effect [18], which is
 208 part of the method itself.

209 The same approach has been applied also in the present study and it is briefly summarized below
 210 for completeness to the reader. It is a four-steps process [19]:

- 211 1. Based on the chord-to-radius ratio of the rotor and the tip-speed ratio, the virtual airfoil due to
 212 flow-curvature effects is defined based on the conformal transformations of Migliore et al. [17].
- 213 2. The virtual airfoil shape is simulated with a code based on panel methods (e.g. XFOIL [34]),
 214 obtaining the pressure coefficient distributions for a wide range of AoAs and a Reynolds number
 215 compatible with that attended on the airfoil. All the pressure coefficient distributions are then
 216 normalized within -1 and +1 by scaling them by their maximum and minimum values. By doing
 217 so, the pressure distributions can be compared only based on the incidence angle (by analyzing
 218 the position of the pressure peaks [19]), with a negligible error on the exact relative speed, which
 219 can be hard to define accurately from CFD calculations.

- 220 3. The pressure coefficient distributions are acquired from CFD calculations at different azimuthal
 221 positions and again normalized within -1 and +1 by scaling them by their maximum and
 222 minimum values.
- 223 4. For every azimuthal position, the pressure coefficient distribution from CFD is compared to all
 224 those calculated for the airfoils. By doing so, the distributions that best fit together can be
 225 highlighted. As discussed, the position along the chord of the pressure peak is mainly used to
 226 define the incidence. This comparison directly provides the estimation of the incidence on the
 227 airfoil. Moreover, by re-scaling the selected pressure profile to match the dimensional one, the
 228 relative speed can be evaluated *a posteriori*.

229

230 3.2 Definition of the relative speed direction on the airfoil

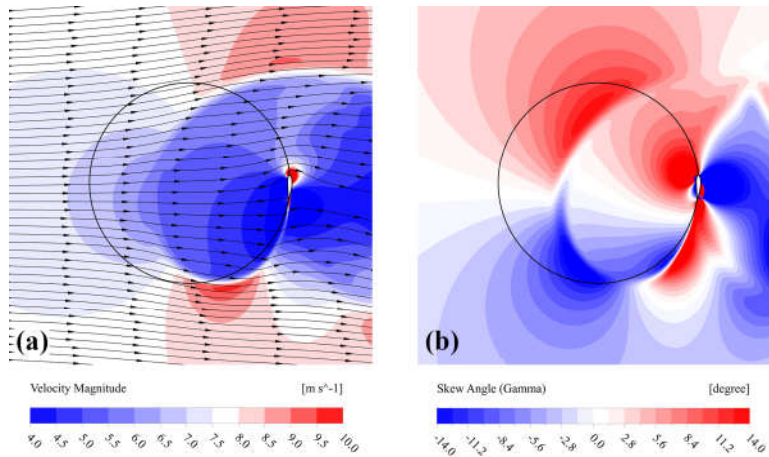
231 If the modulus of relative speed can be obtained following the procedure described above, i.e.
 232 counter-scaling the pressure profile in order to match the intensity of pressure gradients on the
 233 airfoil, no information is given on the direction of the oncoming wind.

234 Low-order models (e.g. BEM models) estimate the relative speed by assuming a simple
 235 reduction of the modulus of undisturbed wind [35], with no modification of its direction (Eq. 2).

236
$$\vec{W} = \vec{\omega}R + \vec{U}(1-a) \quad (2)$$

237 Several experiments (e.g. [36]) and CFD demonstrate, however, that the energy extraction
 238 occurring due to the blade-flow interaction contemporarily induces different slowing down and
 239 deviation of the flow streamlines approaching a Darrieus rotor, making this approach intrinsically
 240 affected by errors. As an example, in Fig. 7a the calculated velocity-field around the transformed
 241 airfoil with $c/R=0.25$ rotating @ TSR=3.1 is reported in terms of modulus and streamlines of the
 242 absolute velocity (U).

243



244

245 **Figure 7 – Transformed airfoil with $c/R=0.25$ @ TSR=3.3, $\beta=270^\circ$: (a) Modulus of the absolute wind speed and**
 246 **streamlines; (b) Skew angle γ .**

247

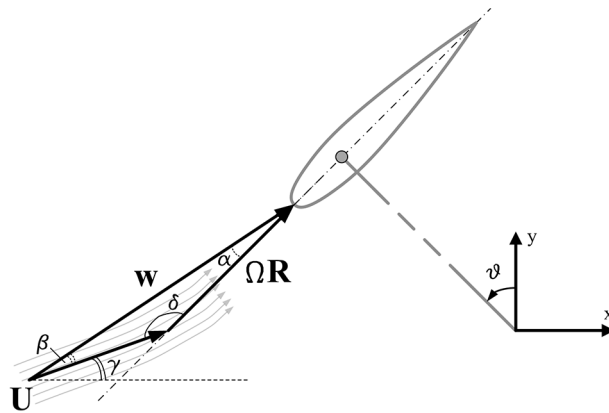
248 Upon examination of the figure, it is apparent that the flow is strongly modified when
 249 approaching the blade orbit, even if a single rotating airfoil is present (i.e. the rotor has a very low
 250 solidity). The undisturbed wind at 8 m/s (neutral color in the figure) cannot reach the airfoil in any
 251 point of the revolution. A remarkable drop in the velocity can be instead noticed, together with a
 252 deflection of the streamlines.

253 To overcome the BEM limitation of simply assuming a reduction of the absolute wind velocity, a
 254 novel approach was here defined.

255 Based on the generic velocity triangle of Fig. 8, it is indeed apparent that the peripheral speed is
 256 a priori known, both in modulus and direction. Moreover, as discussed before, the modulus of the

257 relative speed can be properly estimated based on the analysis of the pressure coefficient
258 distribution on the airfoil. To completely define the velocity triangle, at least the direction of the
259 absolute wind speed must be then given.

260



261

262

263

Figure 8 – Definition of the relative speed on the airfoil.

264 The best estimation of the skew angle γ can be obtained by the computed flow field considering
265 an azimuthal position in which the local flow on the blade only slightly affects the streamlines
266 curvature. By doing so, the deflection of the absolute speed can be estimated to be that induced
267 globally by the energy extraction taking place within the entire rotor.

268 As an example, in Fig. 7b, the same flow field of Fig. 7a is described in terms of local skew
269 angle of the absolute wind speed. As one may notice, the solidity of the rotor makes it work
270 somehow like a porous media, with a specular deflection of the streamlines with respect to the
271 central one, connecting the azimuthal positions of 90° and 270° .

272 With the proposed approach, the velocity triangle on the blades can be then fully described,
273 allowing the detailed analysis of the flow around the airfoils with the conventional lumped
274 parameters approach typical of 1D aerodynamics.

275

276 3.3 Limitations of the approach

277 As discussed in literature [32], the validity of the approach for the determination of the effective
278 AoA on the airfoils unfortunately ceases as soon as the flow is separated around the turbine blades.
279 In these conditions, no reliable blade pressure distribution can be obtained with XFOIL and therefore
280 no comparison can be made from CFD to XFOIL to define the flow incidence on the airfoil itself.
281 Transposing this limitation into an azimuthal range, depending of the airfoil and the TSR, this
282 makes the method working approximately between $\vartheta = -10^\circ$ and $\vartheta = +50^\circ$. Beyond this range, the high
283 angles of attack makes the airfoils work in stalled conditions. Moreover, around $\vartheta = 180^\circ$, where
284 theoretical AoAs are again reduced, the interaction with the macro-vortices detached around $\vartheta = 90^\circ$
285 actually makes the airfoils not experiencing attached flow anymore.

286 Focusing on the estimation of the skew angle of the wind velocity, limitations are here imposed
287 by the assumption that the airfoil is sufficiently far from the considered azimuthal position not to
288 alter the analyzed flow field. In addition, the presence of macro-vortices makes the local
289 determination of γ nearly impossible in a large portion of the blades motion. Again, the most
290 accurate estimations can be made approximately between $\vartheta = -10^\circ$ and $\vartheta = +60^\circ$, then within the same
291 range available for the AoA calculation.

292 Lastly, the entire approach is soundly more accurate in case of a single rotating blade, in which
293 the interaction of other blades does not affect the oncoming flow on the blade itself. However, once
294 the physics of the phenomena have been assessed, the results can be transposed to any Darrieus
295 turbine of arbitrary solidity.

4. Results and discussion

Fig. 9 reports the calculated virtual incidence VI for all the considered airfoils and TSRs as a function of the azimuthal angle of the blade. Results are also compared to the theoretical expectations by Migliore in the same conditions.

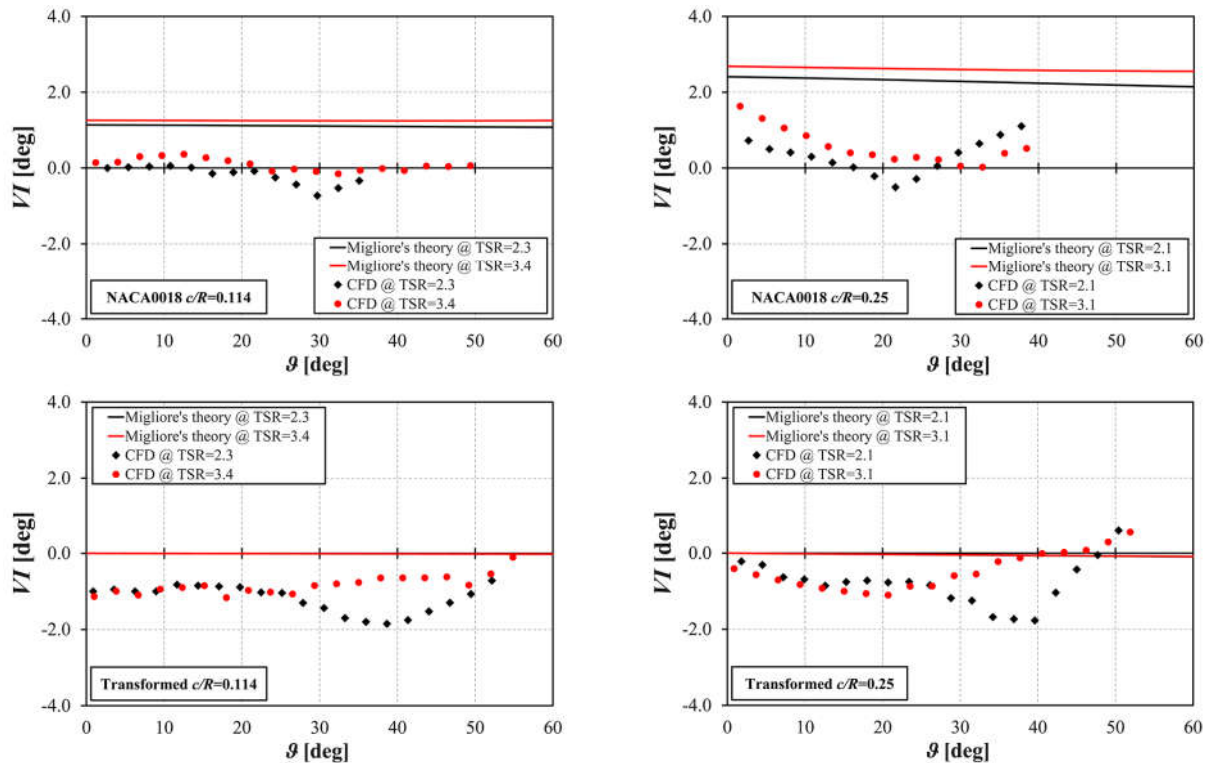
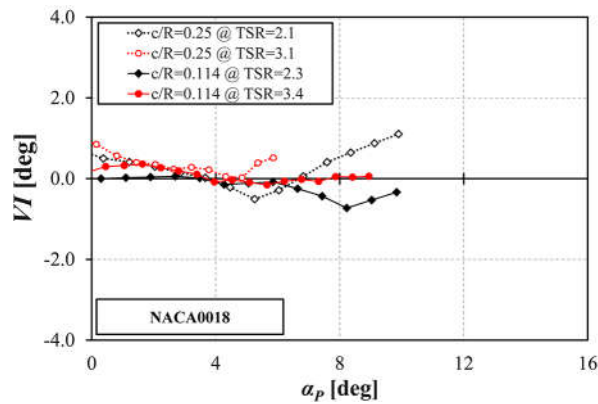


Figure 9 – Virtual Incidence (VI) as a function of the azimuthal position of the blade for all the tested configurations compared to Migliore's theoretical expectations.

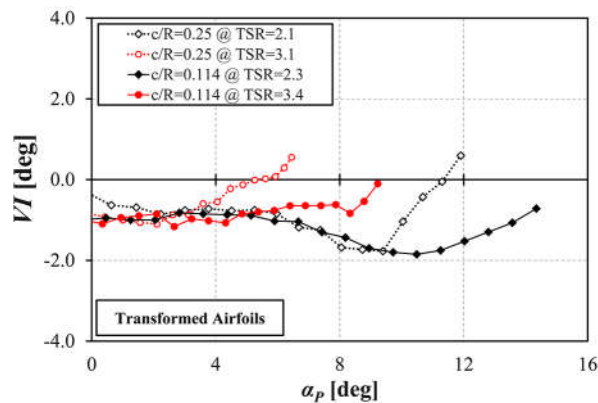
Upon examination of the figure, some relevant markups can be done:

- Calculated VI has the same physical trend than theoretical estimations, being constantly higher for the NACA0018 airfoil than the transformed ones. Moreover, the virtual incidence increases as the chord-to-radius ratio increases. At a fixed c/R , it also slightly increases with the TSR, with an anticipated rise towards high AoAs. The influence of the turbine's parameter (c/R and TSR) are evident especially for the NACA0018 profiles. On the contrary, the transformed profiles are less sensitive to these parameters since the thickness distribution is symmetric with respect to the blade trajectory, which has the same curvature of the camber line.
- With respect the purely theoretical study of Migliore, calculated values are constantly $1^\circ \div 2^\circ$ lower in modulus. This evidence can be probably related to the fact that Migliore did not assume any induction factor (i.e. slow down) of the wind speed, which is instead experienced in reality due to the energy extraction connected to aerodynamic blade-flow interaction. Moreover, the calculated trends are less smooth since the error in the computation of VI values depends on the accuracy of the estimation of various quantities (e.g. α_P , W and γ), which can be easily altered.
- Absolute values appear quite small, but in reality their influence is thought to be absolutely non negligible, as discussed for example in Ref. [35]. In general, where no reliable information of the full azimuthal trend is given, a mean value for VI is supposed to anyhow improve the accuracy of theoretical estimations [16].

323 In order to compare the physical behavior of the airfoils, however, the trend vs. the azimuthal
 324 angle is not appropriate as actually referring to different turbine dimensions. To more directly focus
 325 on the airfoils, in Fig. 10 and Fig. 11 the trends of VI vs. the incidence angles experienced by the
 326 airfoils themselves are reported for the NACA0018 and the transformed profiles, respectively.
 327



328
 329 **Figure 10 – Virtual Incidence (VI) as a function of the AoA for the NACA0018 airfoils in all tested**
 330 **configurations.**
 331



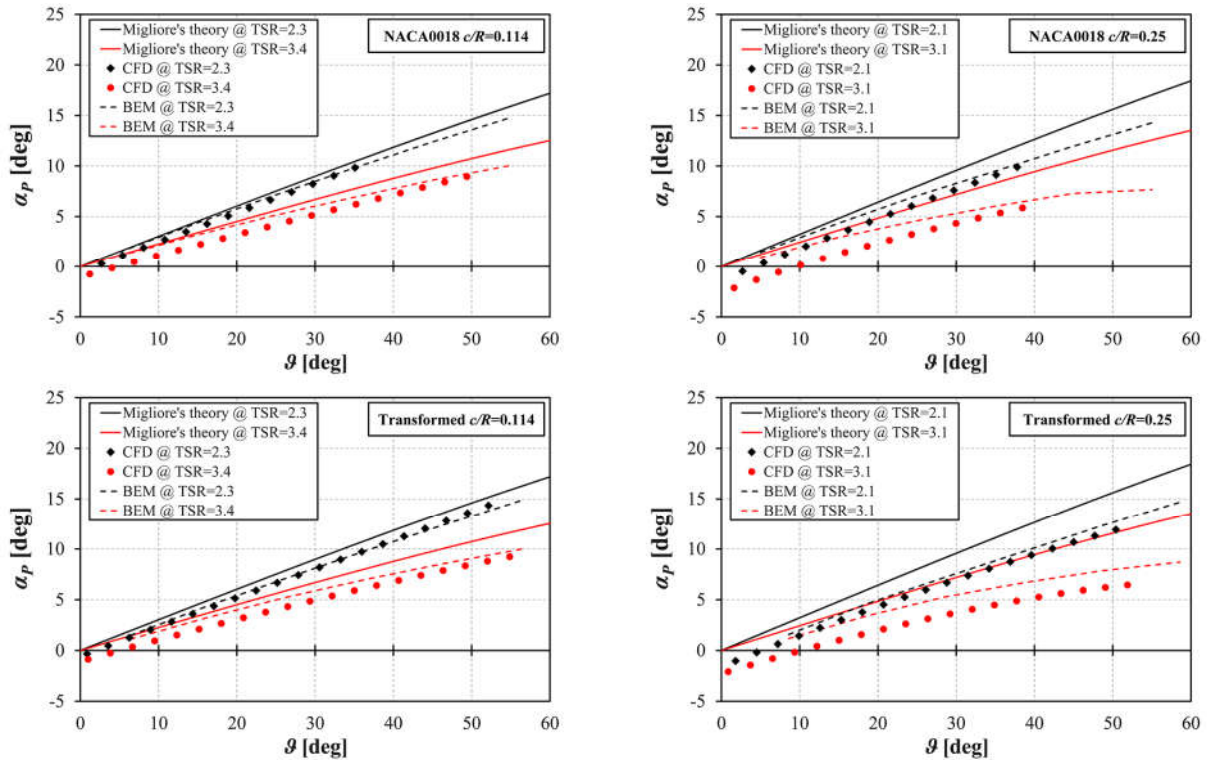
332
 333 **Figure 11 – Virtual Incidence (VI) as a function of the AoA for the transformed airfoils in all tested**
 334 **configurations.**
 335

336 Upon examination of the figures, it is apparent that sound agreement was found between the
 337 aerodynamic behavior of the two airfoils families. Moreover, it is worth remarking that the VI
 338 trends are almost identical for the corresponding chord-to-radius ratios for both airfoils, whereas it
 339 is confirmed that also the TSR has an influence on the trend as the same angle of attack is reached
 340 with a different combination of velocity vectors. For both airfoils, the lowest negative peak of VI
 341 is obtained at both lower TSR and c/R values when the profile experience the largest AoAs. On the
 342 other hand, for the smallest AoAs the values are almost identical.

343 Another set of relevant outcomes is then related to the predicted trend of AoAs as a function of
 344 the turbine rotation. This information is indeed of capital relevance to understand if and how BEM
 345 codes can be predictive of the real performance of a rotor (provided that the proper aerodynamic
 346 coefficients are selected [32]).

347 Figure 12 reports the calculated AoA trends for all the tested configurations. In the graphs, CFD
 348 data are compared to the theoretical expectations of Migliore and to those obtained with a modern
 349 BEM code, i.e. the *VARDAR* code of the Department of Industrial Engineering of the University of
 350 Florence. In detail, the *VARDAR* code has been specifically developed for H-Darrieus wind
 351 turbines using an improved version of a *Double Multiple Streamtubes Approach with Variable*
 352 *Interference Factors* [13]. The Glauert's correction for the BEM theory has been taken into account
 353 with the most recent improvements, together with the corrections due to blades finite Aspect Ratio,

354 using the Lanchester-Prandtl model. In order to increase the accuracy of the aerodynamic
 355 estimations, a specific sub model to account for the dynamic stall has been provided, following the
 356 Paraschivoiu's adaptation to the DMS approach described in; at the same time, the stream tube
 357 expansion along the flow path was considered. For additional details on the code please refer to
 358 Refs. [11,37]. The prediction capabilities of the VARDAR code have been validated during a
 359 several-years' experience in the design of real H-Darrieus rotors, constantly obtaining good
 360 agreement between simulations and experiments.
 361



362
 363 **Figure 12 – AoA as a function of the azimuthal position of the blade for all the tested configurations compared to**
 364 **Migliore's theoretical expectations and BEM simulations.**

365 Results are again very interesting. In detail, all the configurations confirmed that:

- 367 ■ Migliore's estimations made without accounting for an induction factor poorly predict the AoAs
 368 calculated with CFD, with a spread overestimation of the absolute values and a steeper increase
 369 trend.
- 370 ■ The BEM code, even if using the simplified assumption of Eq. 2, predicted quite accurately the
 371 AoA trends.
- 372 ■ As attened [18], the BEM predictions are as accurate as the chord-to-radius ratio is low and
 373 then the flow curvature effects are reduced. In particular, it is apparent that in all $c/R=0.25$
 374 configurations BEM simulations still overestimated the AoA at any azimuthal position.

375 To more clearly understand this behavior, Figure 13 finally reports the skew angle γ of the
 376 absolute wind speed as a function of the azimuthal angle for all of the analyzed configurations.
 377

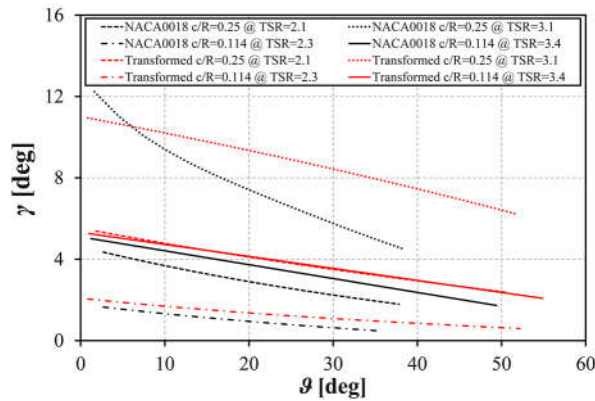


Figure 13 – Skew angle γ as a function of the azimuthal angle for the transformed airfoils in all tested configurations.

Figure 13 clearly highlights that in the configurations at high c/R ratio, where BEM predictions are poorer, the oncoming wind is more strongly deflected due to the virtual porosity of the rotor. In these conditions, the assumption of only a modulus reduction of the wind velocity leads to a bigger error in the AoA estimations and then on the performance prediction. This is probably one of the main reasons of poorer accuracy of BEM codes for high-solidity turbines [13]. As a visual confirmation, Fig. 14 reports the comparison of the contour plots of the calculated skew angles for the transformed airfoils in the same azimuthal position with $c/R=0.114$ and $c/R=0.25$, respectively. Once again, it is readily noticeable that the more solid turbine imposes a stronger deflection to the oncoming flow, with very high γ angles, especially around $\theta=0^\circ$ and $\theta=180^\circ$.

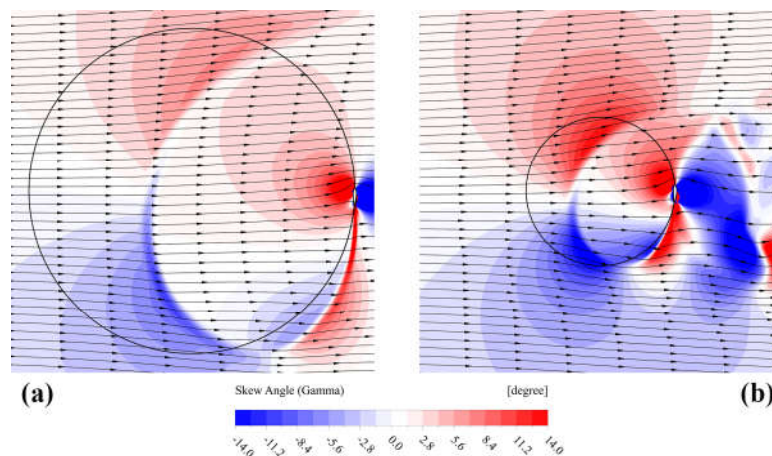


Figure 14 – Calculated skew angles for the transformed airfoils in the same azimuthal position with: (a) $c/R=0.114$; (b) $c/R=0.25$.

5. Conclusions

In the present study, CFD simulations were carried out on a NACA0018 and two airfoils generated by the NACA0018 as to compensate the virtual camber expected in VAWTs with $c/R = 0.114$ and 0.25 .

Numerical results were then analyzed with two novel numerical approaches, which provided proper estimations for the angle of attack on the airfoils and the relative speed in modulus and direction.

These data were then used to calculate the Virtual Incidence imparted on the blades due to their motion in a curvilinear flow, i.e. the difference between the angle of attack really experienced by

404 the airfoil and the flow angle (the angle between the relative velocity and the airfoil's chord) in the
405 same point.

406 Results confirmed that the blades indeed experience a virtual variation in the AoA with respect
407 to theoretical expectations based on the surrounding flow field. In the azimuthal angles range were
408 the proposed approach is applicable, CFD results agreed with the general trends of the original
409 theory even if the absolute values were found to be generally $1^{\circ}\div 2^{\circ}$ lower than theoretical ones. In
410 particular, it was proved that: 1) VI values were higher for the NACA0018 airfoil than the
411 transformed ones; 2) the virtual incidence increases as the chord-to-radius ratio increases; 3) at a
412 fixed c/R , VI also slightly increases with the TSR.

413 In addition, the analysis demonstrated that the wind flow oncoming on a Darrieus rotor is in
414 general strongly deflected by the turbine, with more pronounced values as far as the solidity
415 increases. Notwithstanding this, it was shown that low-order methods, like BEM codes, actually
416 provide quite reliable estimations of the local AoA even if obtained by the incorrect assumption of a
417 simple reduction of the wind velocity modulus.

418 Finally, it is worth remarking that the presented results are of remarkable interest for a further
419 development of BEM codes. If previous works demonstrated that, in case of high chord-to-radius
420 ratios, the airfoils coefficients of virtually transformed airfoils must be considered in the
421 simulations, it was here proved that further correction should be provided to account for the virtual
422 incidence in order to properly match the real performance of the airfoils.

423 Acknowledgments

424 We would like to thank Prof. Ennio Antonio Carnevale of the University of Florence for
425 supporting this research program.

426 Nomenclature

427 Acronyms

428	AoA	Angle of Attack
429	BEM	Blade Element Momentum
430	CFD	Computational Fluid Dynamics
431	HAWTs	Horizontal Axis Wind Turbines
432	SST	Shear Stress Transport
433	TSR	Tip-Speed Ratio
434	U-RANS	Unsteady Reynolds-Averaged Navier-Stokes
435	VAWTs	Vertical Axis Wind Turbines

436

437 Greek symbols

438	α	Angle of Attack (symbol)	[deg]
439	β	Angle Between the Wind Speed and the Relative Speed	[deg]
440	γ	Skew Angle of the Wind Velocity	[deg]
441	δ	Angle Between the Wind Speed and the Peripheral Speed	[deg]
442	ϑ	Azimuthal Angle	[deg]
443	ω	Specific Turbulence Dissipation Rate	[1/s]
444	Ω	Revolution Speed	[m/s]

445

446 Latin symbols

447	A	Turbine's Swept Area	[m ²]
448	c	Blade Chord	[m]
449	D	Rotor Diameter	[m]
450	k	Turbulence Kinetic Energy	[m ² /s ²]

451	R	Rotor Radius	[m]
452	Re_θ	Momentum Thickness Reynolds Number	[-]
453	U	Undisturbed Wind Speed	[m/s]
454	VI	Virtual Incidence	[deg]
455	w	Relative Speed	[m/s]
456	y^+	Dimensionless Wall Distance	[-]
457			

459 **References**

- 460 [1] Kirke BK, Evaluation of self-starting vertical axis wind turbines for standalone applications.
461 Ph.D. thesis, Griffith University, Gold Coast (Australia); 1998.
- 462 [2] Levent Bilir, Mehmet İmir, Yılser Devrim, Ayhan Albostan, An investigation on wind energy
463 potential and small scale wind turbine performance at İncek region – Ankara, Turkey, Energy
464 Conversion and Management, Volume 103, October 2015, Pages 910-923, ISSN 0196-8904,
465 <http://dx.doi.org/10.1016/j.enconman.2015.07.017>.
- 466 [3] Luai M. Al-Hadhrami, Performance evaluation of small wind turbines for off grid
467 applications in Saudi Arabia, Energy Conversion and Management, Volume 81, May 2014,
468 Pages 19-29, ISSN 0196-8904, <http://dx.doi.org/10.1016/j.enconman.2014.01.064>.
- 469 [4] Mertens S. Wind Energy in the Built Environment. Brentwood (UK): Multi-Science; 2006.
- 470 [5] Syngellakis K. Urban wind turbines: Development of the UK market. Proc. of the European
471 Wind Energy Conference 2006, February 27-March 2, Athens (Greece); 2006
- 472 [6] Balduzzi F, Bianchini A, Ferrari L. Microeolic turbines in the built environment: influence of
473 the installation site on the potential energy yield. Renewable Energy 2012;45:163-174.
474 DOI: 10.1016/j.renene.2012.02.022
- 475 [7] Balduzzi F, Bianchini A, Carnevale EA, Ferrari L, Magnani S. Feasibility analysis of a
476 Darrieus vertical-axis wind turbine installation in the rooftop of a building. Applied Energy
477 2012;97:921–929. DOI: 10.1016/j.apenergy.2011.12.008
- 478 [8] Altan BD, Atılgan M, An experimental and numerical study on the improvement of the
479 performance of Savonius wind rotor. Energy Conversion and Management 2008;49(12):3425-
480 3432. DOI: 10.1016/j.enconman.2008.08.021
- 481 [9] Bhuyan S, Biswas A. Investigation on self-starting and performance characteristics of simple
482 h and hybrid H-Savonius vertical axis wind rotors. Energy Conversion and Management
483 2014;87:859-867. DOI: 10.1016/j.enconman.2014.07.056
- 484 [10] Willy Tjiu, Tjukup Marnoto, Sohif Mat, Mohd Hafidz Ruslan, Kamaruzzaman Sopian,
485 Darrieus vertical axis wind turbine for power generation I: Assessment of Darrieus VAWT
486 configurations, Renewable Energy, Volume 75, March 2015, Pages 50-67, ISSN 0960-1481,
487 <http://dx.doi.org/10.1016/j.renene.2014.09.038>.
- 488 [11] Bianchini A, Ferrara G, Ferrari L, Design guidelines for H-Darrieus wind turbines:
489 Optimization of the annual energy yield. Energy Conversion and Management 2015;89:690-
490 707. DOI: 10.1016/j.enconman.2014.10.038
- 491 [12] Aslam Bhutta MM, Hayat N, Farooq AU, Ali Z, Jamil ShR, Hussain Z, Vertical axis wind
492 turbine – A review of various configurations and design techniques. Renewable and
493 Sustainable Energy Reviews 2012;16(4):1926-1939. DOI: 10.1016/j.rser.2011.12.004
- 494 [13] Paraschivoiu I, Wind Turbine Design with Emphasis on Darrieus Concept. Polytechnic
495 International Press, Canada; 2002.
- 496 [14] Simão Ferreira CJ, van Bussel G, van Kuik G. An analytical method to predict the variation in
497 performance of a H-Darrieus in skewed flow and its experimental validation. Proc. of the
498 European Wind Energy Conference, February 27-March 2, 2006, Athens (Greece); 2006.
- 499 [15] Bianchini A, Ferrara G, Ferrari L, Magnani S, An improved model for the performance
500 estimation of an H-Darrieus wind turbine in skewed flow. Wind Engineering 2012;36(6):667-
501 686. DOI: 10.1260/0309-524X.36.6.667
- 502 [16] Balduzzi F, Bianchini A, Maleci R, Ferrara G, Ferrari L. Blade design criteria to compensate
503 the flow curvature effects in H-Darrieus wind turbines. Journal of Turbomachinery
504 2015;137(1):1-10. DOI: 10.1115/1.4028245
- 505 [17] Migliore PG, Wolfe WP, Fanucci JB, Flow curvature effects on Darrieus turbine blade
506 aerodynamics. Journal of Energy 1980;4(2):49-55. DOI: 10.2514/3.62459

- 507 [18] Bianchini A, Balduzzi F, Rainbird J, Peiro J, Graham JMR, Ferrara G, Ferrari L, On the
508 Influence of Virtual Camber Effect on Airfoil Polars for Use in Simulations of Darrieus Wind
509 Turbines. *Energy Conversion and Management*;106(December 2015):373-384.
510 doi:10.1016/j.enconman.2015.09.053.
- 511 [19] Bianchini A, Balduzzi F, Ferrara G, Ferrari L, A computational procedure to define the angle
512 of attack on airfoils rotating around an axis orthogonal to flow direction. Paper submitted for
513 publication to *Journal of Turbomachinery*.
- 514 [20] Hua Yang, Wenzhong Shen, Haoran Xu, Zedong Hong, Chao Liu, Prediction of the wind
515 turbine performance by using BEM with airfoil data extracted from CFD, *Renewable Energy*,
516 Volume 70, October 2014, Pages 107-115, ISSN 0960-1481,
517 <http://dx.doi.org/10.1016/j.renene.2014.05.002>.
- 518 [21] Young-Tae Lee, Hee-Chang Lim, Numerical study of the aerodynamic performance of a
519 500 W Darrieus-type vertical-axis wind turbine, *Renewable Energy*, Volume 83, November
520 2015, Pages 407-415, ISSN 0960-1481, <http://dx.doi.org/10.1016/j.renene.2015.04.043>
- 521 [22] Balduzzi F, Bianchini A, Maleci R, Ferrara G, Ferrari L, Critical issues in the CFD simulation
522 of Darrieus wind turbines. *Renewable Energy* 2016;85:419-435.
523 DOI: 10.1016/j.renene.2015.06.048
- 524 [23] Balduzzi F, Bianchini A, Gigante FA, Ferrara G, Campobasso MS, Ferrari L, Parametric and
525 Comparative Assessment of Navier-Stokes CFD Methodologies for Darrieus Wind Turbine
526 Performance Analysis. Proc. of the ASME Turbo Expo 2015, Montreal, Canada, June 15-19,
527 2015. DOI: 10.1115/GT2015-42663
- 528 [24] Ansys, Inc., 2013, *Fluent Theory Guide*, release 14.5. 4.
- 529 [25] László Daróczy, Gábor Janiga, Klaus Petrasch, Michael Webner, Dominique Thévenin,
530 Comparative analysis of turbulence models for the aerodynamic simulation of H-Darrieus
531 rotors, *Energy*, Available online 24 August 2015, ISSN 0360-5442,
532 <http://dx.doi.org/10.1016/j.energy.2015.07.102>.
- 533 [26] Maître T, Amet E, Pellone C, Modeling of the Flow in a Darrieus Water Turbine: Wall Grid
534 Refinement Analysis and Comparison with Experiments. *Renewable Energy* 2013;51:497–
535 512. DOI: 10.1016/j.renene.2012.09.030
- 536 [27] Raciti Castelli M, Englaro A, Benini E, The Darrieus Wind Turbine: Proposal for a New
537 Performance Prediction Model Based on CFD. *Energy* 2011;36(8):4919–4934. DOI:
538 10.1016/j.energy.2011.05.036
- 539 [28] Bianchini, A., Balduzzi, F., Rainbird, J., Peiro, J., Graham, J M.R., Ferrara, G. and Ferrari, L.,
540 2015, “An Experimental and Numerical Assessment of Airfoil Polars for Use in Darrieus
541 Wind Turbines. Part 2 - Post-Stall Data Extrapolation Methods,” *Journal of Engineering for*
542 *Gas Turbines and Power* 2016;138(3). DOI: 10.1115/1.4031270
- 543 [29] Menter FR, Two-Equation Eddy-Viscosity Turbulence Models for Engineering Applications.
544 *AIAA J.* 1994;32(8):1598–1605.
- 545 [30] Langtry RB, Menter FR, Correlation-based transition modeling for unstructured parallelized
546 computational fluid dynamics codes. *AIAA Journal* 2009;47(12):2894–2906.
- 547 [31] Lanzafame R, Mauro S, Messina M, 2D CFD modeling of H-Darrieus wind turbines using a
548 transition turbulence model. *Energy Procedia* 2014;45:131-140.
- 549 [32] Bianchini A, Balduzzi F, Rainbird J, Peiro J, Graham JMR, Ferrara G, Ferrari L, An
550 Experimental and Numerical Assessment of Airfoil Polars for Use in Darrieus Wind
551 Turbines. Part 1 - Flow Curvature Effects. *Journal of Engineering for Gas Turbines and*
552 *Power* 2016;138(3). DOI: 10.1115/1.4031269.
- 553 [33] Guntur S, Sørensen NN, Evaluation of several methods of determining the angle of attack on
554 wind turbine blades. Proc. of The science of Making Torque from Wind 2012, Oldenburg,
555 Germany, 09-11 October 2012.
- 556 [34] XFOIL User Guide, available online at: <http://web.mit.edu/drela/Public/web/xfoil>, last access
557 02/10/2014

- 558 [35] Bianchini A, Ferrara G, Ferrari L, Pitch Optimization in Small-size Darrieus Wind Turbines,
559 paper accepted for publication in Energy Procedia 2015.
- 560 [36] Vermeulen P, Builtjes P, Dejjer J, Bueren G, An experimental study of the wake behind a
561 full-scale vertical-axis wind turbine. TNO Report 79-06118, 1979.
- 562 [37] Bianchini A, Ferrari L, Magnani S, Start-up behavior of a three-bladed H-Darrieus VAWT:
563 experimental and numerical analysis. Proc. of the ASME Turbo Expo 2011, Vancouver
564 (Canada), June 6-10; 2011. DOI: 10.1115/GT2011-45882